Dalton Transactions

PAPER

View Article Online
View Journal | View Issue

Cite this: *Dalton Trans.*, 2015, **44**, 9538

Rod-like β-FeOOH@poly(dopamine)–Au–poly(dopamine) nanocatalysts with improved recyclable activities

Ya Mao,[a] Wanquan Jiang,*[a] Shouhu Xuan,[b] Qunling Fang,*[c] Ken Cham-Fai Leung,[d] Beng S. Ong,[d] Sheng Wang[a] and Xinglong Gong*[b]

Received 6th March 2015,
Accepted 8th April 2015

DOI: 10.1039/c5dt00913h

www.rsc.org/dalton

A novel rod-like β-FeOOH@poly(dopamine)–Au–poly(dopamine) nanocomposite is developed for recyclable catalysis. Firstly, the rod-like β-FeOOH template was coated *in situ* by a layer of poly(dopamine) (PDA) to form a core/shell nanostructure. Then the negatively charged Au nanocatalysts were well-immobilized onto the periphery of the β-FeOOH@PDA nanorod. To protect the Au nanocrystals from leaching during the catalytic reactions, another PDA layer was coated onto the above particles to form a sandwich-like PDA–Au–PDA shell on the β-FeOOH rod core. The reduction of Rhodamine B (RhB) was introduced as a model reaction to evaluate the catalytic activity of the as-prepared nanocomposites. It was found that the catalytic rate sharply increased with an increasing amount of the nanocatalyst. Benefitting from the thin outer layer of PDA, the recyclability of the nanocatalyst dramatically increased. After five times of catalytic reaction, the activity was maintained as high as 98.3%, while the β-FeOOH@PDA–Au showed it to be retained at only 73.4%.

1. Introduction

Nanocomposites with a well-defined core/shell structure can connect different components together to give novel multifunctional materials and even elevate their practical performances due to the synergistic effects.[1–3] Besides the composition, shape,[4] size,[5] and structures[6] exert a high influence on their practical applications. Since the anisotropic nanostructure exhibits various attractive intrinsic properties, much effort has been applied to develop novel functional one-dimensional core/shell nanocomposites. During the past few years, several defined structures such as dumbbells,[7] rods,[8] wires,[9] *etc*. have been reported and they presented high performance in biological, optical, catalysis, and energy applications.

Nanocatalysts have been demonstrated to be more active than the bulk materials due to their smaller sizes, larger surface areas and more exposed crystal facets. To increase their stabilities in various applications, they were usually immobilized on different substrates to improve the recyclability.[10–13] The coupling of the nanocatalyst with nanocarriers to form core/shell nanostructures effectively facilitates both the separation and recycling. Therefore, a variety of polymers,[14] carbon materials,[15] silica,[16,17] metal organic frameworks[18] and magnetic substrates[19] have been introduced previously. Very recently, it has been reported that the nanocatalysts also inevitably met leaching, leading to activity loss during the repeated reactions.[20,21] To further improve the stability of the nanocatalysts, another protecting layer was introduced onto the surface of the core/shell nanocatalysts. For example, by using the surface etching method, Fe_3O_4@SiO_2@Au@porous-SiO_2 microspheres were developed and they exhibited higher recyclability than Fe_3O_4@SiO_2@Au.[22] Similarly, Fe_3O_4@SiO_2@Pd nanocatalysts could also be coated with a layer of porous-SiO_2 through the CTAB templating method.[23]

Besides the porous inorganic material, polymers were other candidates used to form a good protecting layer. Yin *et al.*[24] grafted a magnetic carrier with a thick layer of poly(*N*-isopropylacrylamide) (p-NIPAM), in which the nanocrystals can be *in situ* confined within the polymer network. Apparently, the high activity and stability of the Au nanocatalysts were attributed to the strong complexation between the nanocrystals

[a]*Department of Chemistry, Collaborative Innovation Center of Suzhou Nano Science and Technology, University of Science and Technology of China (USTC), Hefei 230026, PR China. E-mail: jiangwq@ustc.edu.cn; Fax: +86-551-63600419; Tel: +86-551-63607605*
[b]*CAS Key Laboratory of Mechanical Behavior and Design of Materials, Department of Modern Mechanics, USTC, Hefei 230027, PR China. E-mail: gongxl@ustc.edu.cn; Fax: +86-551-63600419; Tel: +86-551-63600419*
[c]*School of Medical Engineering, Hefei University of Technology, Hefei 230009, PR China. E-mail: fql.good@hfut.edu.cn; Fax: +86-551-62904353; Tel: +86-551-62904353*
[d]*Department of Chemistry and Institute of Creativity, Hong Kong Baptist University, Kowloon, Hong Kong SAR, China*

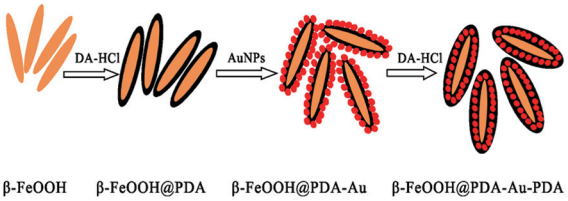

Scheme 1 Synthetic procedure of the β-FeOOH@PDA–Au–PDA nanostructure.

and the polymer matrix. Similarly, the Pd nanocrystals could also be stabilized within the partly carbonized polyaniline shell.[25] Among the various polymer coatings, poly(dopamine) (PDA) has attracted increasing interest because it exhibits strong adhesion on any organic and inorganic substrates,[26–28] showing high hydrophilicity of the controllable coating surface,[29] as well as possessed amino groups which could be directly used as linking bridges for loading other substances through electrostatic attraction. Very recently, Duan *et al.*[30] have reported the synthesis of Au@Ag@PDA core/shell particles by utilizing the redox couple between dopamine and Ag^+ on the Au nanocrystals. It was found that the PDA-coated nanocatalysts survived many reaction cycles without a large drop of the catalytic activities. Clearly, by taking advantages of the strong adhesive property and the ability to direct the seeded growth of metallic nanocrystals, novel nanocomposites with nanocatalysts protected by the PDA shells would be more favorable.

In this work, a simple method has been developed for the preparation of the anisotropic β-FeOOH@PDA–Au–PDA with rod-like β-FeOOH cores and sandwich-like PDA–Au–PDA shells. As depicted in Scheme 1, as soon as the β-FeOOH nanorods were harvested by the condensation reflux method, they were wrapped with a thin PDA layer through the ethanol-mediated oxidative method.[31] Then, the surface of the core/shell particles was decorated with Au NPs by the *in situ* redox approach. Finally, another interfacial polymerization of dopamine was conducted to form sandwich-like PDA–Au–PDA shells. By undertaking the reduction reaction of RhB as a model, the catalytic activities of the as-prepared β-FeOOH@PDA–Au–PDA nanorods were evaluated. Since the outer PDA layer was thin, it not only protected the AuNPs from aggregating and falling off the inner PDA surface, but also improved the reusability of the nanocomposites. Moreover, this method also can be extended to synthesize other kinds of nanocatalysts.

2. Experimental section

2.1. Materials

Iron(III) chloride ($FeCl_3{\cdot}6H_2O$), polyvinylpyrrolidone (PVP, 30 kDa), 3-hydroxytyramine hydrochloride (DA-HCl), ethanol (EtOH), trihydroxymethyl aminomethane (Tris), hydrochloric acid (HCl), gold(III) chloride ($HAuCl_4$), sodium tetrahydridoborate ($NaBH_4$), sodium hydroxide (NaOH), acetic acid (CH_3CHOOH), Rhodamine B dye (RhB), and other chemicals were bought from Sinopharm Chemical Reagent Co. Ltd (SCRC). They were of analytical grade and used without further purification. Deionized water was used during the whole experiment.

2.2. Preparation of the rod-like β-FeOOH@PDA–Au–PDA

Firstly, rod-like β-FeOOH was prepared according to a hydrothermal method. Typically, iron(III) chloride (4 mmol) and polyvinylpyrrolidone (1.0 g) were dissolved in 40 mL H_2O. Then, the resulting mixture was transferred to an oil bath and stirred at 85 °C for 10 h, and the mixture turned into an earthy-yellow suspension. The resulting solids were isolated by centrifugation in water and ethanol. The product was then collected and dried in a vacuum.

For the preparation of β-FeOOH@PDA core/shell nanorods, 20 mg of the as-prepared β-FeOOH was dispersed in a mixture of 20 mL Tris (pH = 8.5) and 40 ml ethanol. Then 15 mL of a DA-HCl aqueous solution (0.67 mg mL^{-1}) was added under stirring, and the mixture was continuously stirred at room temperature for 24 h. During the process, the mixture turned from yellow to olive due to the oxidation and polymerization of dopamine. After separation from the solution and rinsing with water and ethanol, the product was dried in a vacuum.

The synthesis of β-FeOOH@PDA–Au was conducted by using a simple electrostatic attraction method. Firstly, acetic acid (0.4 mL) was added to the ethanolic dispersion of β-FeOOH@PDA (5 mg mL^{-1}, 2 mL) and the resulting mixture was subjected to ultrasound at room temperature for approximately 30 min. Subsequently, an aqueous solution of AuNPs with an average diameter of 4 nm was prepared according to literature procedures.[32] In brief, 40 mL $HAuCl_4$ (2.5×10^{-4} mol L^{-1}) and sodium citrate (2.5×10^{-3} mol L^{-1}) aqueous solution was mixed in a beaker, then 7.5 mL of a $NaBH_4$ solution (6.1×10^{-4} mol L^{-1}) was added rapidly under vigorous stirring. The solution turned bright red after the addition of $NaBH_4$, indicating the formation of citrate modified AuNPs. Finally, the positively charged β-FeOOH@PDA was added to the freshly prepared AuNP solution under vigorous stirring at room temperature for 30 min. The AuNPs were electrostatically attracted on the surface of the β-FeOOH@PDA to form a purple β-FeOOH@PDA-Au solution. After rinsing with water and ethanol, a dry powder form of the product was obtained in a vacuum.

The synthesis of the β-FeOOH@PDA–Au–PDA was similar to the above method. 20 mg of β-FeOOH@PDA–Au was mixed in a mixture of 20 mL Tris (pH = 8.5) and 40 mL ethanol. Then a DA-HCl (0.67 mg mL^{-1}, 15 mL) aqueous solution was added to perform the reaction for 24 h. Subsequently, a black powder was isolated by centrifugation, and washed with water and ethanol three times. After treatment in a vacuum at 40 °C for 12 h, the product β-FeOOH@PDA–Au–PDA was obtained.

2.3. Catalytic properties of the β-FeOOH@PDA–Au–PDA

To investigate the catalytic activity, reduction of RhB with $NaBH_4$ was chosen as the model reaction. Typically, a certain amount of the specific catalyst was added into the RhB solution which contained RhB (20 mL, 2.5×10^{-5} mol L^{-1}), $NaBH_4$ (0.0113 g), and H_2O (10 mL). The color of the mixture vanished gradually from pink to colorless, indicating the successful reduction of RhB. By examining the characteristic absorption of RhB at 553.5 nm as time went on, we could track the concentration variations of RhB. After the reaction was accomplished, the nanocatalysts were collected by centrifugation for the subsequent catalysis. Here, the β-FeOOH@PDA–Au composites with the same Au contents were tested to evaluate the influence of the outer ultrathin layer of PDA on the reusability as well as the catalytic efficiency. The procedure was similar to the above experiments. The mass percentages of β-FeOOH@PDA–Au–PDA and β-FeOOH@PDA–Au were 14.70% and 14.72%, respectively, which were determined by ICP-AES.

2.4. Characterization

X-ray powder diffraction patterns (XRD) of the samples were obtained with a Japan Rigaku DMax-γA rotating anode X-ray diffractometer equipped with graphite monochromatized Cu Kα radiation (λ = 0.154178 nm). Transmission electron microscopy (FE-TEM) images were obtained on a JEM-2100F with an accelerating voltage of 200 kV. The field emission scanning electron microscope (FE-SEM, 20 kV) photographs were taken on a JEOL JSM-6700F SEM. X-ray photoelectron spectra (XPS) were measured on an ESCALAB 250. Infrared (IR) spectra in the wavenumber range 4000–400 cm^{-1} were recorded with a TENSOR Model 27 Fourier transform infrared (FT-IR) spectrometer using a KBr wafer. Thermogravimetric (TG) analysis was conducted on a DTG-60H thermogravimetric instrument, samples were analyzed in alumina pans at a heating rate of 10 °C min^{-1} to 700 °C under the atmosphere of air flowing at 50 mL min^{-1}. The Au contents of the products were determined on an Optima 7300DV inductive coupled plasma atomic emission spectrometer (ICP-AES). The UV-vis spectra were recorded on a TU-1901 spectrophotometer.

3. Results and discussion

Fig. 1 shows the typical TEM images of the products obtained in different reaction steps. As shown in Fig. 1a, it was found that the average length of the β-FeOOH nanorods was approximately 260 nm and the aspect ratio is about 4.5. Due to the relatively monodisperse nature, the β-FeOOH nanorods are suitable to be chosen as the core template for preparing various core/shell particle structures. Here, the β-FeOOH could be very easily coated with a uniform layer of an ultrathin PDA shell *via* a simple *in situ* polymerization method. As shown in Fig. 1b, these well-defined β-FeOOH@PDA core/shell nanorods are well dispersed on the Cu grid without any conglomeration. The average thickness of the PDA is about 2 nm. Next, the freshly prepared AuNP colloid could be immobilized onto the surface of the β-FeOOH@PDA core/shell nanorods by using the electrostatically attracting method. Fig. 1(c) shows the TEM image of uniform AuNP-decorated β-FeOOH@PDA nanorods. Clearly, the dark dots represented the Au nanoparticles with an average size ranging from 4 to 5 nm. Since the strong electrostatic attractions, they were tightly attached onto the nanorods. To further stabilize the attached AuNPs, another PDA layer was coated onto the surface of β-FeOOH@PDA–Au nanorods. As shown in Fig. 1d, the core/shell nanostructure was well maintained after the coating of the outer PDA layer. Here, the simple preparation method not only enables good encapsulation but also prevents the aggregation of the nanorods.

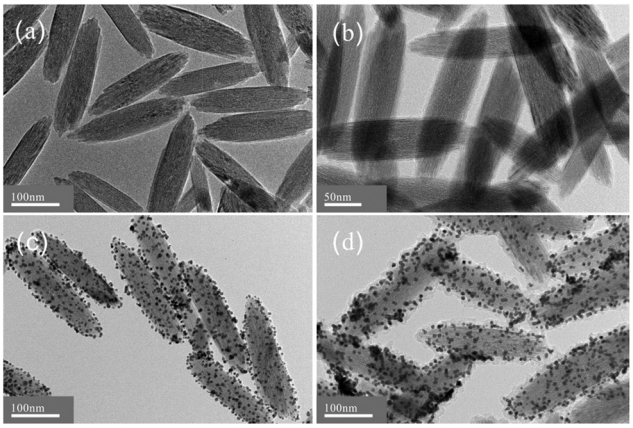

Fig. 1 TEM images of the as-synthesized samples (a) β-FeOOH, (b) β-FeOOH@PDA, (c) β-FeOOH@PDA–Au, and (d) β-FeOOH@PDA–Au–PDA.

The monodispersity and narrow size distribution of the samples prepared at each step could be also clearly observed from the SEM images (Fig. 2). The smooth surface of the particles shown in Fig. 2b can be precisely attributed to the

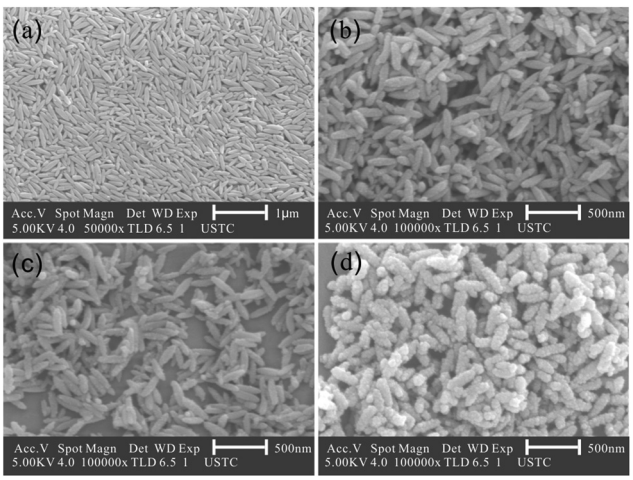

Fig. 2 SEM images of the as-synthesized samples (a) β-FeOOH, (b) β-FeOOH@PDA, (c) β-FeOOH@PDA–Au, and (d) β-FeOOH@PDA–Au–PDA.

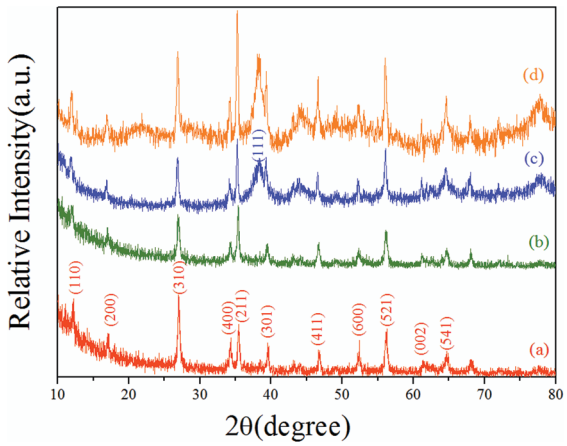

Fig. 3 XRD diffraction patterns of the as-prepared samples (a) β-FeOOH, (b) β-FeOOH@PDA, (c) β-FeOOH@PDA–Au, and (d) β-FeOOH@PDA–Au–PDA.

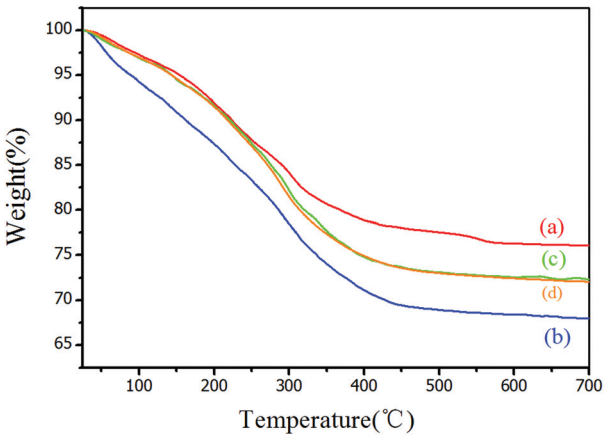

Fig. 4 TG curves of the as-prepared samples (a) β-FeOOH, (b) β-FeOOH@PDA, (c) β-FeOOH@PDA–Au, and (d) β-FeOOH@PDA–Au–PDA.

PDA coating of the β-FeOOH without any aggregation, though conglomeration of nanoparticles has been deemed as one of the main obstacles in the preparation of polymer based nanomaterials. Obviously, due to the supernumerary ultrathin PDA outer layer, the target products shown in Fig. 2d had the roughest surface and the lowest aspect ratio. Based on the above analysis, we could find that all of the samples showed excellent monodispersity and homogeneity, which would be much favored in their future applications.

The crystal structures of the as-prepared core/shell particles were also investigated by XRD. The reflection planes of (110), (200), (310), (400), (211), (301), (411), (600), (521), (002), (541) can be observed in Fig. 3(a), indicating that the pristine nanorod was formed with lattice parameters of a = 10.530 ± 0.005 Å, c = 3.030 ± 0.005 Å, which could be indexed to be the tetragonal phase β-FeOOH (JCPDS 34-1266). Since the PDA layer was thin and non-crystalline, no additional diffraction peaks were found in the β-FeOOH@PDA. As soon as the AuNPs were decorated onto the surface of the β-FeOOH@PDA, a broad peak located at 38° was presented, which was indexed to be the (111) plane of Au. According to the Scherrer equation, the average size of the Au nanoparticles was calculated to be 4.6 nm. This result is in good agreement with the TEM analysis. Moreover the XRD pattern of the β-FeOOH@PDA–Au–PDA is similar to the β-FeOOH@PDA–Au.

The TG curves of the as-prepared samples at each step are shown in Fig. 4. The whole weight loss process was tested between 25 and 700 °C. Because of the decomposition of FeOOH, the residue could be reasonably α-Fe_2O_3 when the temperature was terminated at 700 °C. The weight losses of the samples were 23.87 wt%, 31.98%, 27.65%, and 27.93%, respectively. In comparison with β-FeOOH, β-FeOOH@PDA had an 8.11% more weight loss, due to the presence of PDA encapsulation. Because the AuNPs could not be calcined, the weight loss of the β-FeOOH@PDA–Au was lower than the β-FeOOH@PDA (about 4.33%). Finally, because of the thin outer layer of the PDA shell in β-FeOOH@PDA–Au–PDA, its weight loss was 0.28% higher than β-FeOOH@PDA–Au.

Fig. 5a shows a typical FTIR spectrum of PVP (30 kDa), in which the peaks between 1000 and 1500 cm^{-1} are the characteristic absorptions. The β-FeOOH nanorods were synthesized with a PVP template surfactant, whereas some residue surfactant molecules adsorbed on the nanorods. Thus the peaks at 1654, 2924 and 2854 cm^{-1} that arose due to C=O and C–H vibrations correspond to the residual PVP. The strong absorptions of the β-FeOOH nanorods (Fig. 5b) with vibrational bands at 688 cm^{-1} and 847.5 cm^{-1} could be attributed to Fe-vibration mode. PVP not only attributed to the formation of the rod-like β-FeOOH, but also contributed to the easy coating of PDA on the β-FeOOH cores. In this synthesis, the PDA layer was thin and its adsorption is weak. Thus no additional critical peaks could be found in the β-FeOOH@PDA (Fig. 5c),

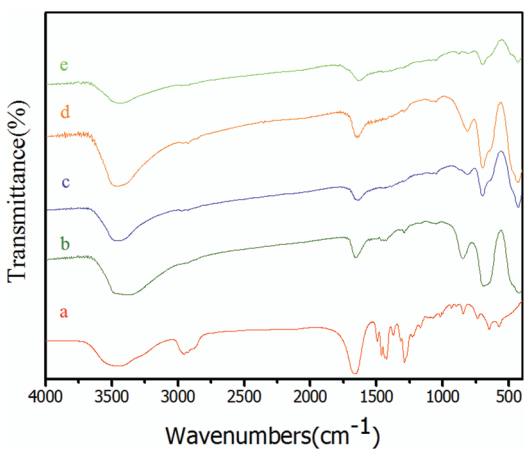

Fig. 5 FT-IR spectra of the as-prepared samples (a) PVPk-30, (b) β-FeOOH, (c) β-FeOOH@PDA, (d) β-FeOOH@PDA–Au, and (e) β-FeOOH@PDA–Au–PDA.

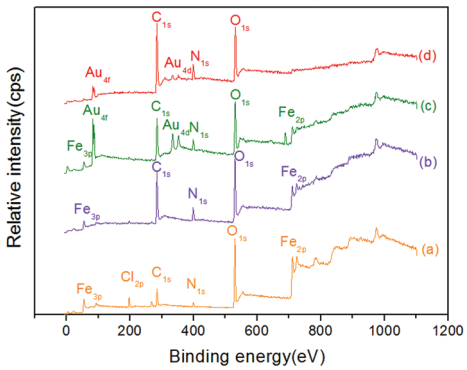

Fig. 6 XPS spectra of the as-prepared (a) β-FeOOH, (b) β-FeOOH@PDA, (c) β-FeOOH@PDA–Au, and (d) β-FeOOH@PDA–Au–PDA.

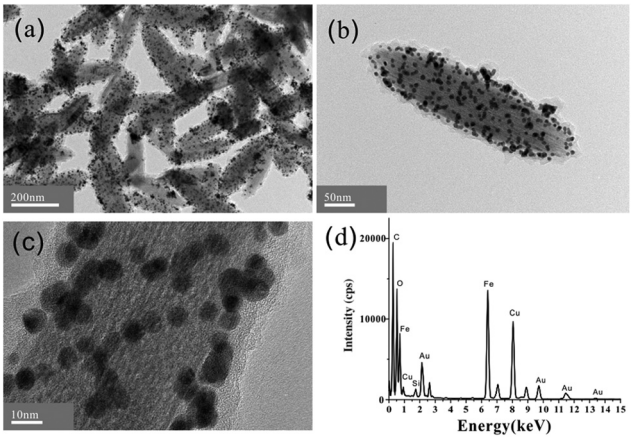

Fig. 7 TEM images of the as-prepared β-FeOOH@PDA–Au–PDA nanorods with different magnifications and the EDS spectrum of the β-FeOOH@PDA–Au–PDA.

β-FeOOH@PDA–Au (Fig. 5d) and β-FeOOH@PDA–Au–PDA (Fig. 5e).

To further analyze the surface state of the as-prepared nanocomposites, XPS was used to characterize the surface elemental components. Fig. 6a shows the XPS spectrum of β-FeOOH with the observation of both Fe and Cl signals, indicating the formation of β-FeOOH with the residue of Cl resulting from the $FeCl_3{\cdot}6H_2O$. After coating with a PDA layer, the relative intensities of C, N, O to Fe shown in Fig. 6b are higher than those in β-FeOOH, demonstrating the thin nature of the PDA shell. Fig. 6c shows the XPS spectrum of β-FeOOH@PDA–Au; a strong Au_{4f} signal was observed, proving the successful adsorption of AuNPs on the surface of β-FeOOH@PDA. However, as soon as the β-FeOOH@PDA–Au was coated with another layer of PDA, the intensity of the Au signal sharply decreased. The detection depth of the XPS is about 10 nm, therefore the Fe $2p^3$ could hardly be found in the XPS spectra for β-FeOOH@PDA–Au–PDA. This result is also in agreement with the above TEM, SEM, and XRD analyses.

The TEM images of the obtained rod-like β-FeOOH@PDA–Au–PDA nanocomposites with different magnifications are shown in Fig. 7. Clearly, the AuNPs are well-distributed on the β-FeOOH@PDA substrates and successfully encapsulated by an ultrathin PDA outer layer. Although some AuNPs aggregates are also present, they are well encapsulated within the PDA shell. Fig. 7c depicts the typical high magnification TEM image of the β-FeOOH@PDA–Au–PDA nanorods. Clearly, most of the Au nanoparticles are well dispersed within the PDA shell separately and the PDA protected them from leaching in the solution. The energy-dispersive X-ray spectroscopy (EDS) analysis of the products shows that the Fe, C, O, and Au elements existed in the nanocomposites, which indicated the presence of β-FeOOH and Au in the product.

3.1. Catalytic properties of the as-prepared β-FeOOH@PDA@Au@PDA nanorods

AuNPs are stable metal nanoparticles, and they present fantastic performances for their size-related electronic and optical properties together. They can be widely applied in electronics, photonics, catalysis and biotechnology. Recently, the Au catalysis for various organic reactions, such as aerobic alcohol oxidation in water,[33] the reduction of the rhodamine B (RhB) dye in the presence of $NaBH_4$,[34] the epoxidation of propylene,[35] the oxidation of CO[36] and so on, has attracted increasing research interest. In this work, the β-FeOOH@PDA–Au–PDA nanorods were employed as catalysts for the reduction of RhB in the presence of $NaBH_4$ to evaluate their catalytic activities. The reduction of RhB was chosen because the concentration changes of RhB could be easily monitored by using UV-vis absorption spectroscopy and no byproducts would be formed.

Fig. 8 shows the typical catalytic performance of the β-FeOOH@PDA–Au–PDA nanorods in the RhB reduction, which could be evidenced by monitoring the maximal absorption of RhB at 553.5 nm. Clearly, with increasing reaction time, the content of the RhB sharply decreased, indicating a clear catalytic activity of the nanorods. Here, the nanocatalyst

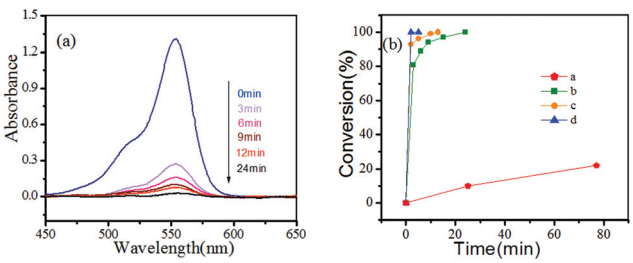

Fig. 8 (a) UV-vis spectra of the reduction of RhB during the reduction catalyzed by β-FeOOH@PDA–Au–PDA composites. [RhB] = 1.67×10^{-5} mol L^{-1}, [$NaBH_4$] = 1×10^{-2} mol L^{-1}, $[Au]_0$ = 1.88×10^{-5} mol L^{-1}. The arrow marked the increase of reaction time, showing the gradual reduction of RhB with β-FeOOH@PDA–Au–PDA catalysts. (b) Plot of conversion (%) of RhB *versus* time (*t*, min) at different concentrations of the Au nanocatalyst (a) $[Au]_0$ = 0 mol L^{-1}, (b) $[Au]_0$ = 1.88×10^{-5} mol L^{-1}, (c) $[Au]_0$ = 2.25×10^{-5} mol L^{-1}, (d) $[Au]_0$ = 2.6×10^{-5} mol L^{-1}. $[RhB]_0$ = 1.67×10^{-5} mol L^{-1} and $[NaBH_4]_0$ = 1×10^{-2} mol L^{-1} remained constant.

is important for the reduction reaction. In the absence of the nanocatalyst, the reduction of RhB proceeded very slowly and the RhB possessed only 30% conversion within 100 min with an excess of $NaBH_4$. Whereas, as soon as appropriate amounts of β-FeOOH@PDA–Au–PDA nanorods were added to the reaction system, the color of the reaction system changed gradually from pink to colorless. Fig. 8(a) shows the UV-vis absorption spectra of the RhB reaction system catalyzed by β-FeOOH@PDA–Au–PDA. Apparently, the maximal absorption of the RhB dye decreased gradually as time went on, demonstrating that the reduction of RhB proceeded. With increasing catalyst content, the reaction time sharply decreased. Moreover, the reduction rate decreased slowly over time, which could be ascribed to pseudo-first-order kinetics that had been reported before.[37]

The catalytic activity of the β-FeOOH@PDA–Au was also investigated in this work. For easy comparison, the content of the β-FeOOH@PDA–Au was tuned to keep the Au concentration similar to the β-FeOOH@PDA–Au–PDA during the catalysis. As shown in Fig. 9(a), the reaction rate of β-FeOOH@PDA–Au was a little quicker than β-FeOOH@PDA–Au–PDA under the same reaction conditions. According to the previous reports,[34,38] in the catalyzed reduction reaction of RhB in the presence of excess $NaBH_4$, the AuNPs could receive electrons donated by the nucleophile hydride of $NaBH_4$ and then the electrophilic RhB dyes would easily capture the electrons delivered by AuNPs because of the intimate contact between RhB and AuNPs. Owing to the existence of the non-conductive outer layer of PDA, electron transportation was impeded between the AuNPs and RhB. Consequently, the degradation of RhB catalyzed by β-FeOOH@PDA–Au–PDA was a little slower than that in the β-FeOOH@PDA–Au case.

The recyclability of the nanocatalysts was also studied to evaluate their catalytic performance. As supported by Fig. 9(b), after five recycles, no remarkable change in the catalytic activity was detected in the case of β-FeOOH@PDA–Au–PDA nanorods. The RhB's conversion rate only decreased from 100% to 98.3%, indicating a good stability over time. However, the catalytic activity of β-FeOOH@PDA–Au critically decreased after five recycles and the RhB's conversion rate changed from 100% to 73.4%, which may be corresponding to the leaching of the nanocrystals during the repeated nanocatalysis reactions. Unfortunately, it was not possible to monitor the Au leaching by ICP due to the Au content being lower than the detection limit. In this work, the content of the Au element and other reaction conditions were the same for the two reactions, thus the higher cyclability must be attributed to the additional protection of the PDA layer in the β-FeOOH@PDA–Au–PDA nanorods. Although the outer PDA layer slightly inhibited the attachment between Au nanocrystals and the RhB substrate, it prevented the Au nanocatalysts from aggregating and falling off the rod carrier, and thus further improved the stabilities during catalysis recyclization.

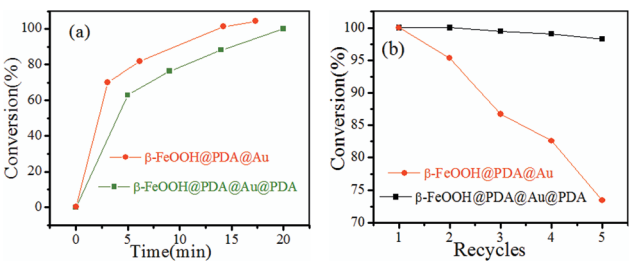

Fig. 9 (a) Conversion of RhB with two types of catalysts: β-FeOOH@PDA–Au–PDA and β-FeOOH@PDA–Au. $[RhB]_0 = 1.54 \times 10^{-5}$ mol L^{-1}, $[NaBH_4]_0 = 0.034$ mol L^{-1}, $[Au]_0 = 2.01 \times 10^{-5}$ mol L^{-1}. (b) Conversion of RhB in five successive cycles of reduction with two types of catalysts: β-FeOOH@PDA–Au–PDA and β-FeOOH@PDA–Au. $[RhB]_0 = 1.54 \times 10^{-5}$ mol L^{-1}, $[NaBH_4]_0 = 0.034$ mol L^{-1}, $[Au]_0 = 2.01 \times 10^{-5}$ mol L^{-1}.

4. Conclusions

In summary, we have demonstrated a facile and reproducible method to synthesize the core/shell β-FeOOH@PDA–Au–PDA nanorods with rod-like β-FeOOH cores and PDA–Au–PDA sandwich shells. Moreover, the catalytic activity of the as-prepared nanocomposites was evaluated by reduction of RhB. Although the reaction rate in the presence of β-FeOOH@PDA–Au–PDA nanorods was a little lower than the β-FeOOH@PDA–Au case, it depicted a much higher stability and recyclability due to the protection of the PDA shell for Au nanocrystals. Since the preparation of the core/shell structures was conducted through a layer-by-layer coating method, various characteristics such as the morphology, shell thickness, and content of the nanocrystals would be controllable. This method would be applied for synthesis of other kinds of sophisticated nanocatalysts.

Acknowledgements

Financial support from the National Natural Science Foundation of China (grant no. 21205026, 11125210) and the Anhui Provincial Natural Science Foundation of China (1408085QA17), and HKRGC-GRF (201412), is gratefully acknowledged.

References

1 K. S. Soppimath, D. C. W. Tan and Y. Y. Yang, *Adv. Mater.*, 2005, **17**, 318.
2 A. S. Zahr, C. A. Davis and M. V. Pishko, *Langmuir*, 2006, **22**, 8178.
3 Y. Yu, M.-Z. Zhang, J. Chen and Y.-D. Zhao, *Dalton Trans.*, 2013, **42**, 885.
4 Y. J. Wang, D. Wang, Q. Fu, D. Liu, Y. Ma, K. Racette, Z. G. He and F. Liu, *Mol. Pharmaceutics*, 2014, **11**, 3766.
5 S. Bashir, A. K. Wahab and H. Idriss, *Catal. Today*, 2015, **240**, 242.

6 G. Sun, F. X. Qi, S. S. Zhang, Y. W. Li, Y. Wang, J. L. Cao, H. Bala, X. D. Wang, T. K. Jia and Z. Y. Zhang, *J. Alloys Compd.*, 2014, **617**, 192.
7 N. T. Khi, J. Yoon, H. Kim, S. Lee, B. Kim, H. Baik, S. J. Kwon and K. Lee, *Nanoscale*, 2013, **5**, 5738.
8 C. W. Liu, Y. C. Wei, C.-C. Liu and K. W. Wang, *J. Mater. Chem.*, 2012, **22**, 4641.
9 X. H. Lu, M. H. Yu, G. M. Wang, T. Zhai, S. L. Xie, Y. C. Ling, Y. X. Tong and Y. Li, *Adv. Mater.*, 2013, **25**, 267.
10 Y. Zhang, Y. Zhou, Z. Zhang, S. Xiang, X. Sheng, S. Zhou and F. Wang, *Dalton Trans.*, 2014, **43**, 1360.
11 S. H. Joo, J. Y. Park, C. K. Tsung, Y. Yamada, P. D. Yang and G. A. Somorjai, *Nat. Mater.*, 2009, **8**, 126.
12 S. C. Tsang, V. Caps, I. Paraskevas, D. Chadwick and D. Thompsett, *Angew. Chem., Int. Ed.*, 2004, **116**, 5763.
13 W. P. Li, P. Y. Liao, C. H. Su and C. S. Yeh, *J. Am. Chem. Soc.*, 2014, **136**, 10062.
14 R. Nakao, H. Rhee and Y. Uozumi, *Org. Lett.*, 2005, **7**, 163.
15 W. H. Chiang and R. H. Sankaran, *Nat. Mater.*, 2009, **8**, 882.
16 S. H. Xuan, F. Wang, X. L. Gong, S.-K. Kong, J. C. Yu and K. C.-F. Leung, *Chem. Commun.*, 2011, **47**, 2514.
17 B. Sun, X. Z. Feng, Y. Yao, Q. Su, W. J. Ji and C.-T. Au, *ACS Catal.*, 2013, **3**, 3099.
18 H. L. Jiang, T. Akita, T. Ishida, M. Haruta and Q. Xu, *J. Am. Chem. Soc.*, 2011, **133**, 1304.
19 W. Q. Jiang, Y. F. Zhou, Y. L. Zhang, S. H. Xuan and X. L. Gong, *Dalton Trans.*, 2012, **41**, 4594.
20 S. D. Miao, C. L. Zhang, Z. M. Liu, B. X. Han, Y. Xie, S. J. Ding and Z. Z. Yang, *J. Phys. Chem. C*, 2008, **112**, 775.
21 L. Zhou, C. Gao and W. J. Xu, *Langmuir*, 2010, **26**, 11217.
22 J. P. Ge, Q. Zhang, T. R. Zhang and Y. D. Yin, *Angew. Chem., Int. Ed.*, 2008, **47**, 8924.
23 W. Li, B. L. Zhang, X. J. Li, H. P. Zhang and Q. Y. Zhang, *Appl. Catal., A*, 2013, **459**, 65.
24 J. P. Ge, T. Huynh, Y. X. Hu and Y. D. Yin, *Nano Lett.*, 2008, **8**, 931.
25 Q. L. Fang, Q. Cheng, H. J. Xu and S. H. Xuan, *Dalton Trans.*, 2014, **43**, 2588.
26 Z. Y. Xi, Y. Y. Xu, L. P. Zhu, Y. Wang and B. K. Zhu, *J. Membr. Sci.*, 2009, **327**, 244.
27 H. Lee, S. M. Dellatore, W. M. Miller and P. B. Messersmith, *Science*, 2007, **318**, 426.
28 J. H. Jiang, L. P. Zhu, L. J. Zhu, B. K. Zhu and Y. Y. Xu, *Langmuir*, 2011, **27**, 14180.
29 B. Li, W. P. Liu, Z. Y. Jiang, X. Dong, B. Y. Wang and Y. R. Zhong, *Langmuir*, 2009, **25**, 7368.
30 J. J. Zhou, B. Duan, Z. Fang, J. B. Song, C. X. Wang, P. B. Messersmith and H. W. Duan, *Adv. Mater.*, 2014, **26**, 701.
31 Q. Yue, M. H. Wang, Z. K. Sun, C. Wang, C. Wang, Y. H. Deng and D. Y. Zhao, *J. Mater. Chem. B*, 2013, **1**, 6085.
32 N. R. Jana, L. Gearheart and C. J. Murphy, *J. Phys. Chem. B*, 2001, **105**, 4065.
33 J. Han, Y. Liu and R. Guo, *Adv. Funct. Mater.*, 2009, **19**, 1112.
34 S. H. Xuan, Y. X. J. Wang, J. C. Yu and K. C. F. Leung, *Langmuir*, 2009, **25**, 11835.
35 T. Hayashi, K. Tanaka and M. Haruta, *J. Catal.*, 1998, **178**, 566.
36 S. Arrii, F. Morfin, A. J. Renouprez and J. L. Rousse, *J. Am. Chem. Soc.*, 2004, **126**, 1199.
37 L. H. Ai, C. M. Zeng and Q. M. Wang, *Catal. Commun.*, 2011, **14**, 68.
38 Z. J. Jiang, C. Y. Liu and L. W. Sun, *J. Phys. Chem. B*, 2005, **109**, 1730.